The RefIEXAFS station at the GILDA beamline (BM08) of ESRF

Francesco D'Acapito,[a]* Ivan Davoli,[b,c] Paolo Ghigna[b,d] and Settimio Mobilio[e]

[a]European Synchrotron Radiation Facility, GILDA CRG, INFM OGG, 6 Rue Jules Horowitz F-38043, France, [b]Laboratori Nazionali di Frascati dell'INFN, via E. Fermi 40, I-00044 Frascati, Italy, [c]Università di Roma 'Tor Vergata', Dipartimento di Fisica, Via della Ricerca Scientifica 1, Roma I-00133, Italy, [d]Università di Pavia Dipartimento di Chimica-Fisica, Pavia, Italy, and [e]Università 'Roma Tre' Dipartimento di Fisica, Via della Vasca Navale 84, Roma I-00146, Italy. E-mail: dacapito@esrf.fr

The experimental station for measuring X-ray absorption spectra in total reflection geometry operative at the GILDA CRG beamline of ESRF is described. The main features of the station are shown, namely: the possibility of detecting very small signals from thin (a few ML) samples, of depositing thin films under controlled conditions and thermal treating the samples in order to study dynamical processes. Case studies are reported in order to show the performances of the apparatus.

Keywords: instrumentation; X-ray absorption spectroscopy; X-ray total reflection; solid-state reactions; semiconductor nanodots.

1. Introduction

X-rays have a relatively low interaction cross section with matter, so they can be considered as a bulk probe. This is a drawback for surface studies, when information on only the first layers of a surface is needed. However, because the index of reflection of X-rays is lower than 1, the surface sensitivity can be obtained by working in grazing-incidence geometry. In fact, in the X-ray region the refraction index n has the form

$$n = 1 - \delta - i\beta,$$

where δ and β are of the order of 10^{-5}–10^{-6} (James, 1962; Parratt, 1954). From Snell's formulae it is found that for grazing angles φ lower than a critical value φ_c the incoming X-ray beam is totally reflected. The critical angle φ_c depends on the energy and on the electronic density of the material, and is found to be

$$\phi_c = (2\delta)^{1/2} \cong 0.5 - 5\,\text{mrad}.$$

Below the critical angle the refracted beam propagates along the sample surface and the electric field decays exponentially into the sample. The depth $z_{1/e}$ at which the intensity of the refracted beam is reduced by 1/e is a function of the optical constants and of the incident angle. $z_{1/e}$ is given by the following approximated formula,

$$z_{1/e} = \lambda / \left[4\pi\left(\varphi_c^2 - \varphi^2\right)^{1/2}\right],$$

which is valid to within 6% for angles $\varphi < 0.85\varphi_c$. We have verified that this validity limit includes the effects due to the non-zero value of the absorption and to the fine-structure oscillations in the angular range indicated above. On the contrary, on approaching the critical angle further, the effect of absorption must be taken into account and the exact formula (Parratt, 1954) should be used. Typical values for $z_{1/e}$ are of the order of a few tens of angstroms as shown in Fig. 1, making the total reflection geometry ideal for surface studies based on X-rays, such as small- (Levine *et al.*, 1989) and wide-angle scattering (Robach *et al.*, 1999), fluorescence elemental analysis (Comin *et al.*, 1999) and absorption (Heald *et al.*, 1988) experiments.

Here will focus our attention on the X-ray absorption spectroscopy technique. The absorption coefficient μ is related to the imaginary part of the refraction index β by

$$\mu = 4\pi\beta/\lambda$$

and β is related to δ *via* a Kramers–Kronig transformation (James, 1962). Since the reflectivity R depends on both β and δ, for a given incidence angle φ there is a one-to-one relation between $\mu(E)$ and $R(E)$. It is relevant to note that absorption edges and EXAFS oscillations, generally observed in the absorption coefficient spectra, can be clearly observed also by measuring the reflectivity spectra $R(E)$ as a function of the energy (Barchewitz *et al.*, 1978). A major problem in data analysis consists of extracting β from R, separating the contribution coming from δ (anomalous dispersion correction, ADC).

Several methods have been developed to extract the EXAFS function $\chi(k)$ from the reflectivity spectra (Martens & Rabe, 1981; Bosio *et al.*, 1984; Poumellec *et al.*, 1989; Heald, 1992; Borthen & Strehblow, 1995, 1997, and references therein) and would require detailed argument to justify the various approximations adopted. In the simplest case, however, when working with an angle $\varphi < \varphi_c$ (0.8–0.6φ_c) and at energies far from the edge (Pizzini, 1990), the absorption coefficient μ can be approximated by the relation

$$\mu \simeq \frac{1 - R(E)}{1 + R(E)}.$$

Also the fluorescence from the surface layer can be used as an indirect method to measure the absorption coefficient. This method, a valid alternative to the reflectivity measurement when working on concentrated samples at very low incidence angles (Chen & Heald, 1993), is also particularly effective in the study of thin films deposited on surfaces. In this case the fluorescence intensity I_f is given by

$$I_f = I_0 \mu_s z_s \varepsilon (\Omega/4\pi)(T/\sin\varphi),$$

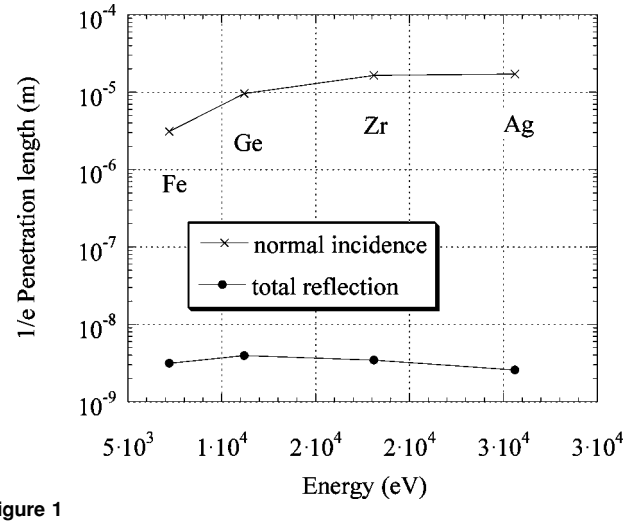

Figure 1
Comparison between the 1/e penetration lengths in a series of bulk elements in normal and total reflection conditions. The calculations were performed at an angle $\varphi = 0.8\varphi_c$ and at an energy 100 eV above the relative K absorption edges to simulate the beam penetration in a typical EXAFS energy range. Values are around tens of μm in the former case and a few nm in the latter case, with a drop of roughly four orders of magnitude when working in total reflection.

where I_0 is the intensity of the incoming beam (photons s^{-1}), μ_s and z_s are the sample absorption coefficient and thickness, respectively ($z_s << z_{1/e}$), ε is the fluorescence yield of the element selected and Ω is the solid angle collected by the detector. Note that in the case of a thin film its contribution to the optical constants of the sampled layer (of the order of $z_{1/e}$) is negligible, as shown by Jiang & Crozier (1997*a*,*b*), so no ADC is needed in this case. The factor T, the transmission factor, is the ratio between the intensity per unit surface of the refracted and incoming beams. Results show that $T = 4$ for $\varphi = \varphi_c$ (ideal interface); $T = 1$ for $\varphi >> \varphi_c$; and $T \rightarrow 0$ for $\varphi << \varphi_c$ (Naudon & Thiaudiere, 1997). In a conventional data collection the same formula holds for $T = 1$, with, typically, $\varphi = 45^\circ$. Therefore, in total reflection mode when $\varphi \simeq 0.2^\circ$ a gain of more than two orders of magnitude can be achieved, owing to this geometrical factor. An additional very important peculiarity of this technique, when dealing with thin films on single-crystal substrates, is that the beam confinement prevents the refracted beam from reaching the substrate, minimizing the disturbing effect of Bragg peaks coming from the substrate.

Examples of experimental apparatus for the collection of ReflEXAFS data, operative on different synchrotron radiation sources like LURE-Orsay (Bosio *et al.*, 1983), NSLS-Upton and CHESS-Ithaca (Heald *et al.*, 1988; Chen, 1989), SSRL-Stanford (Jiang *et al.*, 1988), SRS-Daresbury (Pizzini *et al.*, 1989; Pizzini, 1990; Smith *et al.*, 1995), HASYLAB-Hamburg (Clausnitzer *et al.*, 1989; Hecht *et al.*, 1995), KEK-Tsukuba (Oyanagi, Owen *et al.*, 1995) can be found in the literature.

The ReflEXAFS technique has been shown to be effective when investigating surface problems in different research fields, such as semiconductor physics (Barrett *et al.*, 1990; Oyanagi, Sakamoto *et al.*, 1995; Bayliss *et al.*, 1994; Cheong *et al.*, 2001; Gupta *et al.*, 2000; Wei *et al.*, 2000), ion-implanted materials (Allain *et al.*, 1992; Gibson & Crabb, 1995), sputter deposited thin films (Lutzenkirchen-Hecht & Frahm, 2000), adsorbates on substrates (Charnock *et al.*, 1995; Endo *et al.*, 1999), reactions at electrodes (Bosio *et al.*, 1984; Hecht, Borthen & Strehblow, 1996; Hecht, Frahm & Strehblow, 1996), metal–metal interfaces (Heald *et al.*, 1988; Jiang *et al.*, 1991; Chen & Heald, 1990), glass surfaces (Van Dorssen *et al.*, 1995; Greaves, 1990) and organic layers (Oyanagi *et al.*, 1988; Schlieben & Hormes, 1999).

2. Experimental apparatus

The GILDA CRG beamline (D'Acapito *et al.*, 1998; updated information on the beamline can be found at http://www.esrf.fr/exp_facilities/BM8/handbook/control.html) is installed on a 0.8 T bending magnet of the European Synchrotron Radiation Facility (ESRF) (critical energy $\simeq$ 19 keV). The beamline optics consists of a collimating mirror, a double-crystal sagittally focusing monochromator and a second vertically focusing mirror. The monochromator works in the so-called 'dynamically focusing' mode (Pascarelli *et al.*, 1996), *i.e.* the sagittal bending radius of the second crystal is adjusted at each energy step to keep the focal position fixed on the sample. The parallelism between the two crystals is controlled by a piezo actuator acting on the first crystal and driven by a PID controller (D'Acapito, 1997). Under the working conditions the two crystals are *detuned* from parallelism (usually at 70% of the reflectivity maximum); in this way a high harmonic rejection is achieved as well as an excellent stabilization against vibrations. When using Si(311) as monochromator crystals, the energy range between 5 and 31 keV is covered with an intensity between 10^{10} and 10^{11} photons s^{-1} on the sample.

ReflEXAFS experiments are carried out in a dedicated vacuum chamber containing the sample holder and supporting the detectors for incoming beam normalization, sample reflectivity and fluorescence (Fig. 2). These kinds of measurements require a beam with a small size (50–100 µm), low divergence and stable incidence angle. In order to fulfil these requirements the beam from the monochromator is delimited by a couple of 50 µm-wide tungsten slits, at a distance of 2 m from each other. The first slit is placed in a vacuum chamber upstream of the ReflEXAFS apparatus, the second slit is mounted near the incident beam detector as shown in Fig. 3. 100 µm slits can be used when a high-luminosity configuration is needed. Just after this slit, the beam passes through a metallic foil; various metals are used depending on the energy range investigated, with a typical thickness of 5–0.5 µm (Fig. 3). A large-area Si photodiode (thickness 300 µm) used in photovoltaic mode monitors the foil fluorescence and hence the intensity of the incoming beam. This solution (Gauthier *et al.*, 1995) permits the realization of a high-quality detector that fits into an extremely reduced space, as needed in our case. A second slit, wider than the first (100–200 µm) and placed after the fluorescent foil, is used to clean the beam from undesired scattered radiation. The aperture of the second slit corresponds to less than 1/100 of the solid angle collected by the photodiode, as this sensor reads a typical current of some 10^{-10} A. The intensity of the contaminating beam is thus estimated to correspond to a few pA on the reflectivity detector, *i.e.* 10^{-5}–10^{-4} lower than its typical signals. During RefleEXAFS

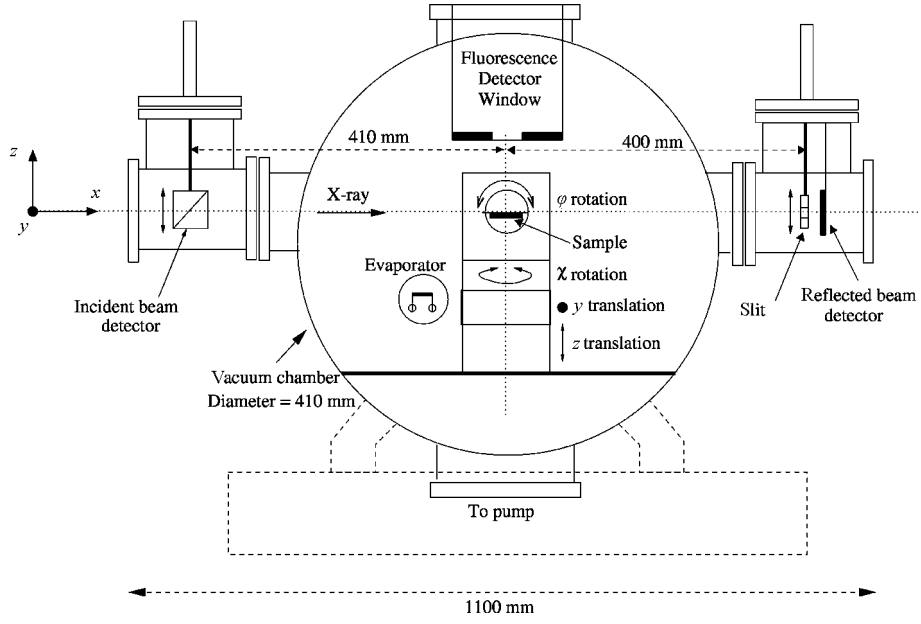

Figure 2
Sketch of the ReflEXAFS vacuum chamber installed at the GILDA beamline. The beam enters from the left and passes through the incident beam detector before hitting the sample. The sample is placed on a holder that provides movements for the horizontal and vertical alignment. Successive 90° rotations about the φ and χ axes permit the sample to be placed in front of the evaporator when required. The reflected beam is read by a photodiode placed after the chamber in the beam path whereas the fluorescence from the sample is read from the top by a 13-element high-purity Ge detector. A further opening for the side placement of the detector is also present but not shown in the drawing for clarity.

measurements the incoming-beam monitor is used also as a sensor for the monochromator feedback system, to provide a very stable beam on the sample ($\Delta I/I \simeq 10^{-3}$).

The sample holder is mounted inside a vacuum chamber, on a mechanical positioning system (Fig. 2) consisting of two goniometers (φ and χ rotations) with axes parallel to the y and z directions, respectively. A translation module is also associated with each rotation axis so that the angle and distance of the sample surface with respect to the beam can be adjusted to set the sample in total reflection condition with the beam polarization vector parallel (the most often used configuration) or perpendicular to the surface.

The beam reflected by the sample is measured by another large-area Si photodiode placed behind the chamber (Fig. 2) and perpendicular to the beam. A 40 μm slit is set across the direct beam during the sample alignment procedure that follows the steps described in the literature (Jiang *et al.*, 1988; Pizzini *et al.*, 1989). Above this slit a wide aperture permits the beam to reach the photodiode; after alignment the slit is lowered to transmit ∼5% of the residual direct beam and the sample angle is varied to collect the reflectivity. The use of a large-area detector for the reflected beam without beam collimation (Jiang *et al.*, 1988; Pizzini *et al.*, 1989; Hecht, Borthen & Strehblow, 1996; Chen, 1989) permits complex coupled motions to be avoided but at the expense of a slight contamination due to fluorescence/diffuse scattering from the sample. In our apparatus the reflectivity range available is roughly four orders of magnitude, similar to that observed in other ReflEXAFS spectrometers (Hecht, Borthen & Strehblow, 1996).

For the *in situ* sample preparation, an oven working up to 1373 K and an evaporator are available. The oven is mounted on a dedicated φ goniometer with angular resolution of 1.2×10^{-2} deg. The sample is placed on a heated holder (length 5 cm), oversized with respect to the typical sample dimensions (length 2 cm) in order to have a temperature profile on the sample as flat as possible. The temperature readout is made by a K-type thermocouple placed inside the sample holder, whereas a second thermocouple, placed near the heater, drives the thermal control system. By performing a 90° rotation of both the φ and χ goniometers (Fig. 2) the sample can be positioned in front of the crucible of the evaporation system. Deposition rates range from a few angstroms to a few tens of angstroms. The thickness of the deposited layer is measured by a quartz balance placed just near the sample holder. Absolute determinations of the film thickness are also possible by measuring X-ray reflectivity *in situ*. After the deposition the film can be heated to induce reactions with the substrate or with a controlled atmosphere present in the chamber. Examples of the possible treatments will be shown in the following section. After the deposition the sample holder can be easily realigned in the beam to the required accuracy.

When thermal treatments are not needed, a high-precision φ rotation stage is available for sample positioning. In this case the sample holder works at room temperature and has an angular resolution of 5×10^{-4} deg; this system also allows EXAFS measurements from multilayer Bragg peaks to be performed (where a high resolved variable angle is needed) as shown by Staub *et al.* (2001).

Fluorescence from the sample is detected by a 13-element high-purity Ge detector coupled to a digital signal processor. This permits the signal detection with an energy resolution of typically 200 eV at the Mn K_α line (E = 5.89 keV) at a total count rate of up to 1 Mcounts s^{-1} on the whole detector. The fluorescent beam reaches the detector through two alternative flanges, one looking at the sample from the top (Fig. 2) and the other from the side. In the *top mounting* geometry the fluorescence from one monolayer coverage is easily detected. In such geometry ∼1/25 of the total solid angle of emission is covered but a contribution of the elastically scattered radiation is also detected. However, it must be noted that when working on surface-deposited films in the total reflection condition the elastic peak is smaller than the fluorescence, even for monolayer-thick samples.

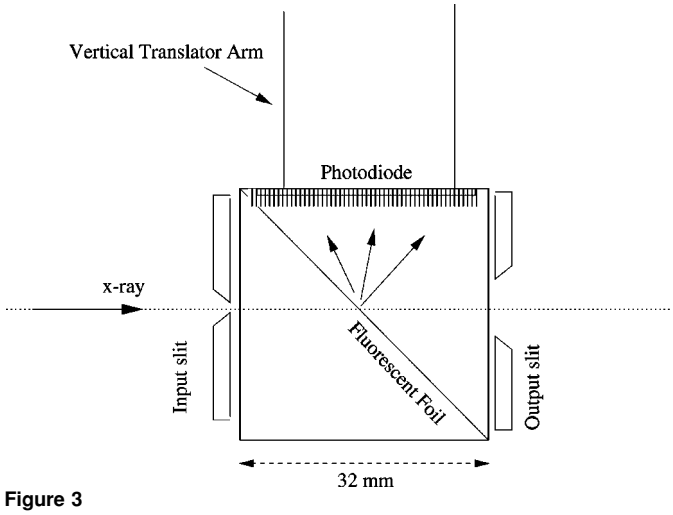

Figure 3
Sketch of the incident-beam detector. The beam is sized by a thin (50–100 μm) slit and hits a fluorescent metallic foil. The component of the foil is chosen depending on the energy region. The X-ray fluorescence induced by the beam is collected by a large-area Si PIN photodiode positioned near the foil. At the end a wider slit (100–200 μm) is used to clean the probe beam from slit scattering and residual fluorescence. The block is mounted on a vertical translator for accurate positioning of the slit on the beam.

3. Case applications

In this section we present some examples of experiments that have been carried out on the presented spectrometer. We firstly present an *in situ* sample preparation where a Ni thin film is deposited and then a chemical reaction where the substrate is thermally induced. The treatment was carried out in the following way: step (1) a 225 Å Ni layer was evaporated onto a single crystal of Al_2O_3 (1–211); step (2) the sample was treated at 973 K for 20 min in a 60 mbar O_2 atmosphere to promote its oxidation to NiO; step (3) final treatment at 1273 K for 9 h to promote the NiO reaction with the substrate. Also the last thermal treatment was performed in a 60 mbar O_2 atmosphere to avoid reduction of the oxide layer. Fig. 4 shows the measured energy-dependent reflectivities obtained by correcting the reflectivity diode readout by its energy-dependent response obtained by an energy scan without the sample. These data were found to be in good agreement with calculations of R based on theoretical scattering factors (Sasaki, 1989). The reflectivity data were then converted to absorption coefficients using the method shown by Poumellec *et al.* (1989). Successive EXAFS data were extracted following the standard procedure (Lee *et al.*, 1981) and are shown in Fig. 5 together with the model compound spectra recorded in transmission mode. Comparison between these spectra permits us to qualitatively determine the phases of the structural transformation: after step (1) a metallic layer is formed, probably made up of small clusters because an appreciable amplitude reduction of the signal is observed in the spectrum. In step (2) the film is oxidized to NiO, and finally it reacts with the substrate to give rise to the $NiAl_2O_4$ spinel in the last thermal treatment, step (3). A complete quantitative analysis of all these steps and of the intermediate phases between steps (2) and (3) is still in progress.

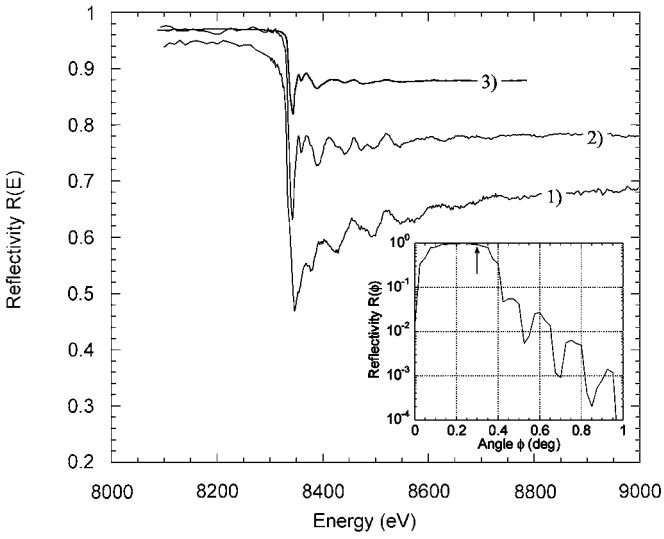

Figure 4
Reflectivities $R(E)$ measured on the 225 Å Ni as-evaporated film (step 1); the oxidized film after 30 min annealing at 973 K in 60 mbar O_2 (step 2); the film after reaction with the substrate induced by a long annealing (9 h) at 1273 K (step 3). The inset shows the angle-dependent reflectivity taken at 8 keV in step (1). The collection angles were 0.30° (marked by an arrow in the inset), 0.25° and 0.22° for steps (1), (2) and (3), respectively. The cusp-like shape in spectrum (1) is the distortion due to anomalous dispersion.

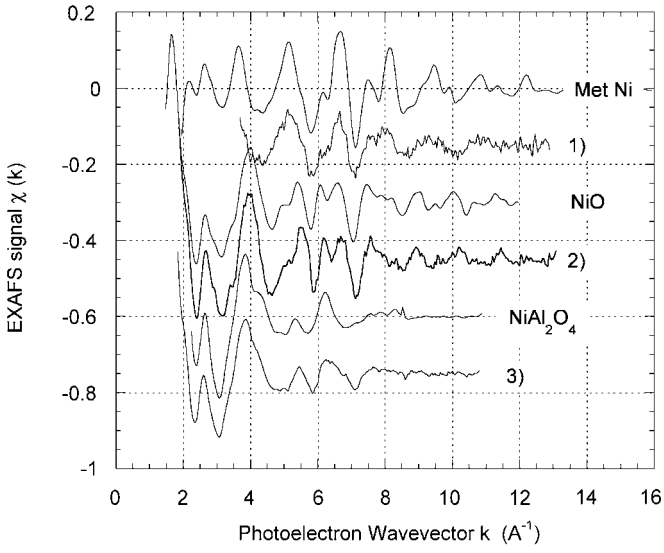

Figure 5
EXAFS spectra of the samples obtained in steps (1), (2) and (3) extracted from the $R(E)$ shown in Fig. 4 making use of the Poumellec method (Poumellec *et al.*, 1989). The reference compounds (metallic Ni, NiO and $NiAl_2O_4$) recorded in transmission mode are also shown as evidence for the various phases of the transformation.

A second field of applications of ReflEXAFS is the structural study of thin layers on a crystalline substrate. When working at high energy, severe problems owing to Bragg peaks from the substrate are encountered. As previously underlined, this can be minimized by limiting the penetration of the probe beam in the substrate. Fig. 6 shows the absorption spectrum of a 2 ML InAs dots layer on a single-crystal GaAs substrate recorded at the In *K*-edge (27940 eV) and collected with the 13-element high-purity Ge detector. The measurements were carried out at an angle near to the critical value as shown in the figure inset, to maximize the fluorescence yield

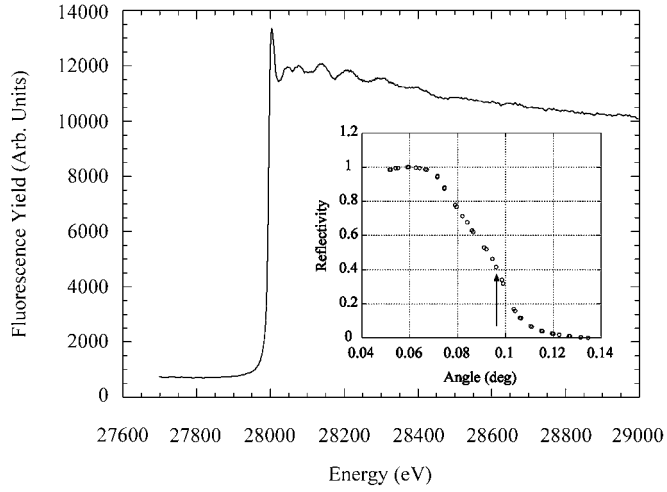

Figure 6
Absorption spectrum of 2 ML InAs on GaAs at the In *K*-edge collected with a 13-element Ge detector and integrating 3 s point^{-1}. Inset: the reflectivity spectrum at 28 keV; the arrow marks the working angle, near the critical value.

keeping the penetration length at a low value (∼200 nm). The data quality is good, showing that spectra from a thin (ML range) sample can be easily obtained even at relatively high energies.

Finally, further examples of investigations carried out using this apparatus can be found in the literature, such as studies on the oxidation of metals (D'Acapito *et al.*, 2000), structure of multilayers (Staub *et al.*, 2001), lipid Langmuir–Blodgett films (D'Acapito, Relini *et al.*, 2002) and semiconductor thin films (D'Acapito, Davoli *et al.*, 2002).

4. Conclusion

We have described the experimental apparatus for ReflEXAFS measurements now operative at the GILDA CRG beamline of the European Synchrotron Radiation Facility. The sample is kept in a vacuum chamber that contains the holder with all the mechanical movements for alignment and an evaporator for sample preparation. The detection system is based on Si PIN photodiodes for the measurement of the incident and reflected beam whereas the fluorescence is read by a 13-element high-purity Ge detector. Typical beam sizes are ∼50 µm and the accessible energy range is between 5 and 31 keV. Case studies on samples prepared *in situ* and on thin films have been shown.

The GILDA beamline is financed by CNR, INFN, INFM. The technical support of F. d'Anca, F. Campolungo, C. Capelli, V. Sciarra, V. Tullio and P. Zandalazini is greatly acknowledged. The authors thank Professor M. G. Proietti for providing the InAs:GaAs spectra and Dr A. Cardelli for writing the ADC routines.

References

Allain, J. L., Regnard, J. R., Bourret, A., Parisini, A., Armigliato, A., Tourillon, G. & Pizzini, S. (1992). *Phys. Rev B*, **46**, 9434–9445.
Barchewitz, R., Cremonese-Visicato, M. & Onori, G. (1978). *J. Phys. C*, **11**, 4439–4445.
Barrett, N. T., Greaves, G. N., Pizzini, S. & Roberts, K. J. (1990). *Surf. Sci.* **227**, 337–346.
Bayliss, S. C., Anstee, P., Hutt, D. A., Zhang, Q., Danson, N., Bates, J. & Waddilove, A. (1994). *J. Appl. Phys.* **76**, 5171–5178.
Borthen, P. & Strehblow, H. H. (1995). *Phys. Rev. B*, **52**, 3017–3019.

Borthen, P. & Strehblow, H. H. (1997). *J. Phys. IV*, C**2**, 187–189.
Bosio, L., Cortes, R., Defrain, A. & Froment, M. (1984). *J. Electroanal. Chem.* **180**, 265–271.
Bosio, L., Cortes, R., Defrain, A. & Gomes da Costa, P. (1983). *Le Vide, les Couches Minces*, **216**, 197–198.
Charnock, J. M., England, K. E. R., Farquar, M. L. & Vaughan, D. J. (1995). *Physica B*, **208**/**209**, 457–458.
Chen, H. (1989). PhD thesis, City University of New York, USA.
Chen, H. & Heald, S. M. (1990). *Phys. Rev. B*, **42**, 4913–4920.
Chen, H. & Heald, S. M. (1993). *J. Appl. Phys.* **73**, 2467.
Cheong, S., Bunker, B., Hall, D. C., Snider, G. L. & Barrios, P. J. (2001). *J. Synchrotron Rad.* **8**, 824–826.
Clausnitzer, M., Pauly, T. & Materlik, G. (1989). *Rev. Sci. Instrum.* **60**, 2436.
Comin, F., Navizet, M., Mangiagalli, P. & Apostolo, G. (1999). *Nucl. Instrum. Methods*, B**150**, 538–542.
D'Acapito, F. (1997). PhD thesis, Université Joseph Fourier, Grenoble, France.
D'Acapito, F., Colonna, S., Pascarelli, S., Antonioli, G., Balerna, A., Bazzini, A., Boscherini, F., Campolungo, F., Chini, G., Dalba, G., Davoli, I., Fornasini, P., Graziola, R., Licheri, G., Meneghini, C., Rocca, F., Sangiorgio, L., Sciarra, V., Tullio, V. & Mobilio, S. (1998). *ESRF Newslett.* **30**, 42–44.
D'Acapito, F., Davoli, I., Castrucci, P. & de Crescenzi, M. (2002). *Surf. Sci.* **518**, 183–191.
D'Acapito, F., Mobilio, S., Cikmacs, P., Merlo, V. & Davoli, I. (2000). *Surf. Sci.* **468**, 77–84.
D'Acapito, F., Relini, A., Emelianov, I., Solari, P., Cavatorta, P., Morante, S., Mincozzi, V., Gliozzi, A. & Rolandi, R. (2002). *Langmuir*, **18**, 5277–5282.
Endo, O., Kiguchi, M., Yokoyama, T., Ito, M. & Ohta, T. (1999). *J. Electroanal. Chem.* **473**, 19–24.
Gauthier, C., Goujon, G., Feite, S., Mouguiline, E., Braicovich, L., Brookes, N. B. & Goulon, J. (1995). *Physica B*, **208**/**209**, 232–234.
Gibson, P. N. & Crabb, T. A. (1995). *Nucl. Instrum. Methods*, B**97**, 495–498.
Greaves, G. N. (1990). *J. Non-Cryst. Solids*, **120**, 108.
Gupta, J. A., Watkins, S. P., Crozier, E. D., Woicik, J. C., Harrison, D. A., Jiang, D. T., Pickering, I. J. & Karlin, B. A. (2000). *Phys. Rev. B*, **61**, 2073–2084.
Heald, S. M. (1992). *Rev. Sci. Instrum.* **63**, 873–878.
Heald, S. M., Tranquada, J. M. & Chen, H. (1988). *Phys. Rev. B*, **38**, 1016–1026.
Hecht, D., Borthen, P. & Strehblow, H. H. (1995). *J. Electroanal. Chem.* **381**, 113–121.
Hecht, D., Borthen, P. & Strehblow, H. H. (1996). *Surf. Sci.* **365**, 263–277.
Hecht, D., Frahm, R. & Strehblow, H. H. (1996). *J. Phys. Chem.* **100**, 10831–10833.
James, R. W. (1962). *The Optical Principles of the Diffraction of X-rays*. Woodbridge: Ox Bow Press.
Jiang, D. T., Alberding, N., Seary, A. J. & Crozier, E. D. (1988). *Rev. Sci. Instrum.* **59**, 60–63.
Jiang, D. T. & Crozier, E. D. (1997*a*). *J. Phys. IV*, C**2**, 247–248.
Jiang, D. T. & Crozier, E. D. (1997*b*). *J. Phys. IV*, C**2**, 249–250.
Jiang, D. T., Crozier, E. D. & Heinrich, B. (1991). *Phys. Rev. B*, **44**, 6401–6409.
Lee, P. A., Citrin, P. H., Eisenberger, P. & Kincaid, B. M. (1981). *Rev. Mod. Phys.* **53**, 769–806.
Levine, J. R., Cohen, J. B., Chung, Y. W. & Geougopoulos, P. (1989). *J. Appl. Cryst.* **22**, 528–532.
Lutzenkirchen-Hecht, D. & Frahm, R. (2000). *Physica B*, **283**, 108–113.
Martens, G. & Rabe, P. (1981). *J. Phys. C*, **14**, 1523–1534.
Naudon, A. & Thiaudiere, D. (1997). *J. Appl. Cryst.* **30**, 822.
Oyanagi, H., Owen, I., Grimshaw, M., Head, P., Martini, M. & Saito, M. (1995). *Rev. Sci. Instrum.* **66**, 5477–5485.
Oyanagi, H., Sakamoto, K., Shioda, R., Kuwahara, Y. & Haga, K. (1995). *Phys. Rev. B*, **52**, 5824–5829.
Oyanagi, H., Yoneyama, N., Ikegami, K., Sugi, M., Kuroda, S. I., Ishiguro, T. & Matsushita, T. (1988). *Thin Solid Films*, **159**, 435–432.
Parratt, L. G. (1954). *Phys. Rev.* **95**, 359–369.
Pascarelli, S., Boscherini, F., d'Acapito, F., Hrdy, J., Meneghini, C. & Mobilio, S. (1996). *J. Synchrotron Rad.* **3**, 147–155.
Pizzini, S. (1990). PhD thesis, University of Strathclide, UK.
Pizzini, S., Roberts, K. J., Greaves, G. M., Harris, N., Moore, P., Pantos, E. & Oldman, R. J. (1989). *Rev. Sci. Instrum.* **60**, 2525–2528.
Poumellec, B., Cortes, R., Lagnel, F. & Tourillon, G. (1989). *Physica B*, **158**, 282–283.
Robach, O., Renaud, G. & Barbier, A. (1999). *Phys. Rev. B*, **60**, 5858–5871.
Sasaki, S. (1989). *Numerical Tables of Anomalous Scattering Factors Calculated by the Cromer and Liebermann Method*, KEK Report 88–14, pp. 1–136. KEK, Tsukuba, Japan.
Schlieben, O. & Hormes, J. (1999). *J. Synchrotron Rad.* **6**, 793–795.
Smith, A. D., Roper, M. D. & Padmore, H. A. (1995). *Nucl. Instrum. Methods*, B**97**, 579–584.
Staub, U., Zaharko, O., Grimmer, H., Horigsberger, M. & d'Acapito F. (2001). *Europhys. Lett.* **56**, 241–246.
Van Dorssen, G. E., Derst, G., Greaves, G. N., Smith, A. D. & Roper, M. (1995). *Nucl. Instrum. Methods*, B**97**, 426–429.
Wei, S., Oyanagi, H., Sakamoto, K., Takeda, Y. & Pearsall, T. P. (2000). *Phys. Rev. B*, **62**, 1883–1888.